Scientia Iranica B (2022) 29(3), 1236–1249

Sharif University of Technology
Scientia Iranica
Transactions B: Mechanical Engineering
http://scientiairanica.sharif.edu

Sensitivity analysis for Walters-B nanoliquid flow over a radiative Riga surface by RSM

A. Shafiq[a], F. Mebarek-Oudina[b,*], T.N. Sindhu[c], and G. Rasool[d]

a. *School of Mathematics and Statistics, Nanjing University of Information Science and Technology, Nanjing 210044, China.*
b. *Department of Physics, Faculty of Sciences, University of 20 Août 1955-Skikda, Skikda, Algeria.*
c. *Department of Statistics, Quaid-I-Azam University 4250 Islamabad 44000, Pakistan.*
d. *Binjiang College, Nanjing University of Information Science and Technology, Wuxi 214105, China.*

Received 11 May 2021; received in revised form 21 September 2021; accepted 6 December 2021

KEYWORDS
Sensitivity analysis;
Walters-B nanofluid;
Newtonian heating;
Moving Riga surface;
Stagnation point flow;
Response surface methodology.

Abstract. In this study, a sensitivity analysis is implemented using response surface strategies to control the Walters-B nanofluid stagnant point flow caused by a Riga surface. An electromagnetic actuator is known as Riga surface. The Buongiorno model is used to construct the mathematical model that includes a Newtonian heating condition as well as radiation effects. Based on the fundamental laws of mass, momentum, and energy, transformation is incorporated to obtain nonlinear ordinary differential equations. To solve the governing system, the numerical shooting approach along with Runge-Kutta scheme is employed to solve the governing system. By considering the response of Local Nusselt Number (LNN) to the variation of input variables, an experimental structure is incorporated by sensitivity analysis. As underlined, the LNN is quite sensitive to radiation number rather than other parameters of interest. Meanwhile, it is indicated that the sensitivity of LNN to Brownian number is reduced as thermophoresis is enhanced, but sensitivity value varies from positive to negative for all the values of Brownian number. It is examined that maximum LNN occurs at a higher level for thermophoresis and for Brownian motion parameters. The results are assumed to provide a tentative guidance for possible lab-based experiments.

1. Introduction

There are many compliant methods including nanoparticle addition to base liquid, rendering surfaces flexible, applying a magnetic field, corrugating surfaces, attaching fin(s), incorporating artificial surface roughness, and adding obstacle(s) for improving heat transfer from thermal devices [1–6]. The study of nanofluids has recently attracted the attention of current researchers owing to the extensive use of numerous processes/industries like engine cooling, machining and electronics, heat exchanger systems, improving the performance of diesel generators and heat transport of chillers, hybrid-powered air conditioners/refrigerators, solar water heating, fuel cells, and other high-consumption energy equipment. Nanofluids, in general, have more thermal characteristics than traditional liquids, which is the reason why they are often referred to as advanced/next-generation heat transport liquids. Thermal engineers have concentrated on nanoliquids due to their essential and insightful characteristics like higher conductivity and larger relative area of nanomaterials. The nanomaterials suspended in the nanoliquid significantly improve

*. *Corresponding author. Tel.: +21 3668305488*
E-mail addresses: oudina2003@yahoo.fr, f.mebarek_oudina@univ-skikda.dz (F. Mebarek-Oudina)

doi: 10.24200/sci.2021.58293.5662

the suspension stability and heat transfer capabilities. Nanofluids enjoy numerous use cases because they can improve heat transfer efficiency as compared to pure fluids. Choi and Eastman [7] pioneered the study of heat transport in nanoliquids. Dispersion of a small number of solid nanomaterials in pure liquid considerably improves its thermal conductivity which in turn leads to the enhancement of the heat transport rate [6]. This has received much recognition and inspired many researchers. There are numerous studies in the literature that have discussed the mechanism underlying the improved heat transport characteristics [8–19]. An outstanding collection of research studies on this matter is accessible through a review of the referenced papers [20–33]. Riga sheet is an electromagnetic actuator. Riga sheets generate electric and magnetic fields that can generate Lorentz force parallel to liquid flow [34]. It is obvious that liquids with high electrical conductivity are significantly affected when a magnetic field is applied. Several researchers have been inspired by this scenario to analyze the liquid flows through Riga sheet. Ahmad et al. [35] considered the dependability of the asymptotic technique to address the impact of strong suction and mixed convective boundary layer flow of nanoliquid through a Riga surface. With the assistance of analytical solutions, Dhif et al. [36] analyzed the thermal examination of the solar collector cum storage system by utilizing a hybrid-nanofluids. Abbas et al. [37] analyzed the importance of Electro-Magneto-Hydrodynamic (EMHD) and bioconvective nanofluid flow toward a porous Riga sheet containing gyrotactic microorganisms. Nadeem et al. [38] employed the MATLAB bvp4c methodology to investigate the nanofluid stagnant point flow via Riga plate through induced magnetic impacts. Ganesh et al. [39] studied two-dimensional nanoliquid flow to achieve an expandable Riga sheet with EMHD impacts by employing shooting numerical techniques. Rasool et al. [40] studied the second-grade nanoliquid flow towards a heated vertical Riga surface. Shafiq et al. [41] investigated thermosoluted Marangoni flow towards a vertical porous Riga sheet. Zhang et al. [42] analyzed the bioconvection flow of nanoliquid through a Riga surface with Darcy-Brinkman-Forchheimer porous medium. Bhatti and Michaelides [43] reported the significance of Arrhenius activation energy concerning bioconvective nanofluid flow on a Riga surface. Shafiq et al. [44] numerically studied the Marangoni flow of carbon nanotubes over a Riga area.

Response Surface Methodology (RSM) is a multivariate optimization approach that employs a variety of statistical and mathematical methods. This method is focused on fitting a polynomial term to experimental data. In general, this approach can be utilized whenever a comeback or set of responses (output variables) is influenced by a number of independent variables (input variables). RSM optimizes the responses at the same time in order to achieve the best system efficiency. Several investigators utilized sensitivity analysis for energy issues via RSM [45,46]. For instance, Bovand et al. [47] employed sensitivity study of a vortex tube refrigerator. They found the highest cold temperature difference in a vortex tube to be the most sensitive to cold orifice diameter than to the inlet pressure or the amount of intake in the nozzle. Rashidi et al. [48] utilized response surface methods to conduct a sensitivity study for nanoliquid flow over an equilateral triangle barrier. They found Local Nusselt Number (LNN) and Skin Friction Coefficient (SFC) sensitive to the solid volume fraction of the nanoliquid in all situations. They also discovered a significant agreement between the findings of computational liquid dynamics study and those of RSM. Shafiq et al. [49] analyzed the sensitivity study of bioconvection tangent hyperbolic nanoliquid over the moving stretched sheet by RSM.

A thorough review of the literature reveals that the sensitivity analysis of the Walters-B nanofluid stagnant point flow induced by a Riga plate has not been studied previously. Therefore, the purpose of the present research work is to study non-Newtonian Walters-B nanofluid flow over stretching Riga plate with Newtonian heating. Buongiorno's model is utilized to investigate the nanofluid features. A mathematical model is suggested for use in the context of partial differential equations. To convert them into similarity equations, appropriate transformation is employed. Numerical solution is sought using Runge-Kutta-Fehlberg (RKF) method via shooting. Moreover, an experimental framework (RSM) is inextricably linked to sensitivity analysis to investigate the dependence of interested output terms over input terms. Interestingly, the authors performed sensitivity scrutiny using the LNN. This research is related to possible rules in future gadget production. To date, such research is novel for the top systematic review discovered.

2. Mathematical formulation

Significance of the stagnant point flow of Walters-B nanoliquid along a stretching Riga plate is investigated. Thermal radiation and Newtonian heating are employed to investigate heat transfer features. Figure 1 shows a schematic depiction of the physical model under consideration. Buongiorno's method is utilized to investigate the nanofluid properties. The governing equation is written in the following under the given assumptions by using Boussinesq approximations:

$$\frac{\partial v}{\partial y} + \frac{\partial u}{\partial x} = 0, \tag{1}$$

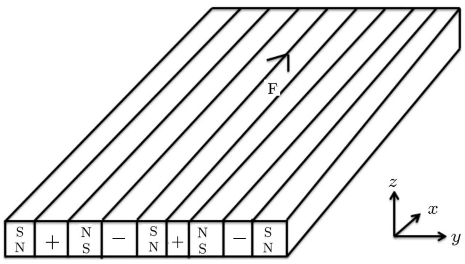

Figure 1. Studied problem of Riga plate.

$$u\frac{\partial u}{\partial x}+v\frac{\partial u}{\partial y}-U_e\frac{dU_e}{dx}=v\frac{\partial^2 u}{\partial y^2}$$

$$-\frac{k_0}{\rho}\left[v\frac{\partial^3 u}{\partial y^3}+u\frac{\partial^3 u}{\partial x\partial y^2}+\frac{\partial u}{\partial x}\frac{\partial^2 u}{\partial y^2}\right.$$

$$\left.-\frac{\partial u}{\partial y}\frac{\partial^2 u}{\partial x\partial y}\right]+\frac{\pi j_0 M_0}{8\rho}\exp\left(-\frac{\pi}{a}y\right), \tag{2}$$

$$v\frac{\partial T}{\partial y}+u\frac{\partial T}{\partial x}=\left(\frac{16\sigma^* T_\infty^3}{3k_1}+K\right)\frac{\partial^2 T}{\partial y^2}$$

$$+\tilde{\tau}\left[\tilde{D}_b\frac{\partial C}{\partial y}\frac{\partial T}{\partial y}+\frac{\tilde{D}_t}{T_\infty}\left(\frac{\partial T}{\partial y}\right)^2\right], \tag{3}$$

$$u\frac{\partial C}{\partial x}+v\frac{\partial C}{\partial y}=\tilde{D}_b\frac{\partial^2 C}{\partial y^2}+\frac{\tilde{D}_t}{T_\infty}\frac{\partial^2 T}{\partial y^2}, \tag{4}$$

$$u\left(x,\,0\right)=U_w(x)=cx,\ v(x,\,0)=0,$$

$$\left.\frac{\partial T\left(x,\,y\right)}{\partial y}\right|_{y=0}=-h_s T\left(x,\,0\right),$$

$$C\left(x,\,0\right)=C_w,u\to U_e(x)=bx,$$

$$T\to T_\infty\quad C\to C_\infty\quad \text{as}\quad y\to\infty. \tag{5}$$

Proper variables are incorporated as follows:

$$v\left(x,\,y\right)=-\sqrt{cv}f\left(\eta\right),$$

$$u\left(x,\,y\right)=cxf'\left(\eta\right),$$

$$\theta=\frac{T-T_\infty}{T_\infty},\quad \theta=\frac{T-T_\infty}{T_\infty},$$

$$\phi=\frac{C-C_\infty}{C_w-C_\infty},\quad \eta=\sqrt{\frac{c}{v}}y. \tag{6}$$

The continuity equation is resolved instantly, whereas the remaining governing equations are reduced to the following forms:

$$f'''+A^2-\left(f'\right)^2+ff''-W_e\left[2f'f'''-\left(f''\right)^2-ff^{(iv)}\right]$$

$$+Q_1\exp\left(-\beta\eta\right)=0,$$

$$f\left(0\right)=0,f'\left(0\right)=1,\quad f'\left(\infty\right)=A, \tag{7}$$

$$\left(1+\frac{4}{3}R_d\right)\theta''+Prf\theta'+Pr\,N_2\theta'\phi'+Pr\,N_1\theta^{2'}=0,$$

$$\theta'(0)=-\delta\left(1+\theta(0)\right),\qquad \theta(\infty)=0, \tag{8}$$

$$\phi''+S_c f\phi'+\frac{N_1}{N_2}\theta''=0,\quad \phi(0)=1,\quad \phi(\infty)=1. \tag{9}$$

Here, the prime designates differentiation with respect to η. The parameters are as follows:

$$A=\frac{b}{c},\quad We=\frac{k_0 c}{\mu_0},\quad \beta=\sqrt{\frac{\pi^2\nu}{a^2 c}},$$

$$Q_1=\frac{\pi j_0 M_0}{8\rho U_w^2},\quad Pr=\frac{\mu_0 c_p}{K},\quad R_d=\frac{4\sigma^* T_\infty^3}{k_1 K},$$

$$Sc=\frac{\nu}{\tilde{D}_b},\quad \delta=h_s\sqrt{\frac{v}{a}},\quad N_2=\frac{\tilde{\tau}\tilde{D}_b\left(C_w-C_\infty\right)}{\upsilon},$$

$$N_1=\frac{\tilde{\tau}\tilde{D}_t}{\upsilon}. \tag{10}$$

The details are given in nomenclature. SFC C_f, LNN Nu_x, and LSHN are as follows:

$$C_f=\frac{\tau_w}{\rho U_w^2},\quad Nu_{\tilde{x}}=\frac{xq_w}{K\left(T_w-T_\infty\right)},$$

$$Sh_{\tilde{x}}=\frac{\tilde{D}_b j_w}{\tilde{D}_b\left(C_w-T_\infty\right)},$$

where the wall heat flux q_w and the wall skin friction τ_w are as follows:

$$\tau_w=\left[\mu_0\frac{\partial u}{\partial y}-k_0\left(u\frac{\partial^2 u}{\partial x\partial y}+v\frac{\partial^2 u}{\partial y^2}+2\frac{\partial u}{\partial x}\frac{\partial u}{\partial y}\right)^3\right]_{y=0},$$

$$q_w=-K\left(\frac{\partial T}{\partial y}\right)_{y=0},\qquad j_w=-\tilde{D}_b\left(\frac{\partial C}{\partial y}\right)_{y=0}. \tag{11}$$

Using Eq. (6), we have:

$$\left(Re_x\right)^{1/2}C_f=\left(1-3We\right)f''\left(0\right), \tag{12}$$

$$\left(Re_{\tilde{x}}\right)^{-1/2}Nu_{\tilde{x}}\delta\left(1+\frac{3}{4}R_d\right)\left(1+\frac{1}{\theta\left(0\right)}\right), \tag{13}$$

$$\left(Re_{\tilde{x}}\right)^{-1/2}Sh_{\tilde{x}}=-\phi'\left(0\right), \tag{14}$$

where $Re_x=cx^2/v$ is the local Re.

2.1. Nonlinear polynomial model

A statistical technique based on a standard non-linear polynomial method may be utilized to evaluate the relationships between the target response variable and the independent input variables.

$$R = r_0 + r_1 A_1 + r_2 B_1 + r_3 C_1 + r_{11} A_1^2 + r_{22} B_1^2 + r_{33} C_1^2 + r_{12} A_1 B_1 + r_{13} A_1 C_1 + r_{23} B_1 C_1. \quad (15)$$

The mathematical model contains one intercept term, three bilinear two-factor terms, three linear terms, and three quadratic terms. Thus, R indicates the LNN response. It is focused on three independent input parameters that are coded by symbols A_1, B_1, and C_1 (radiation, thermophoresis, and Brownian motion numbers, respectively). According to the RSM, 20 runs with 19 DOF (Degrees Of Freedom) are optimal for the selected three stages of variables. These are the low, medium, and high stages including (−1, 0, 1), respectively. Table 1 lists the input variables along with their symbols and levels. Furthermore, in R-programming, Central Composite Design (CCD) is typically utilized for the execution of a numerical or computational experiment. A set of 20 runs of experiments is arranged in terms of $2^F + 2F + P$, in which the number of factors is $F = 3$ and the number of center points is $P = 6$. Table 2 describes the experimental program sequence. The Analysis of Variance (ANOVA) is a statistical technique for determining the importance of the variability performance of defined variables on the RSM model. ANOVA is used to investigate the optimization criterion in the RSM model in terms of model precision, with numerical estimators such as DOF, Sum of Squares (SS), and Minimum Mean Square (MMS) as well as p-value and F-value. The LNN for the ANOVA analysis is shown in Table 3.

Table 4 shows the deterioration coefficients for responses (local Nu) based on the p-value set for the nonlinear polynomial model in Eq. (14). The high p-value is known as statistically insignificant, which implies that no relative change to the output can be noted due to the changes made to the input. On the other hand, it is possible to ignore the term with a low p-value (≤ 0.05), which is statistically significant elsewhere. As a consequence, $A, B, C, A^2, B^2, C^2, AB$, and

Table 1. Experimental variables and their level.

Parameter symbol			Level: Low (−1)	Medium (0)	High (1)
LNN	R_1	A	0.1	0.2	0.3
	N_1	B	0.2	0.4	0.6
	N_2	C	0.2	0.4	0.6

Table 2. Experiment design and response performance of $-\mathrm{Re}_x^{-1/2} Nu_x$.

Runs	Coded value A_1	B_1	C_1	Real values R_d	N_1	N_2	Responses $-\mathrm{Re}_x^{-1/2} Nu_x$
1	−1	−1	−1	0.1	0.2	0.2	0.281664
2	1	−1	−1	0.3	0.2	0.2	0.347108
3	−1	1	−1	0.1	0.6	0.2	0.289786
4	1	1	−1	0.3	0.6	0.2	0.35714
5	−1	−1	1	0.1	0.2	0.6	0.296965
6	1	−1	1	0.3	0.2	0.6	0.370294
7	−1	1	1	0.1	0.6	0.6	0.264525
8	1	1	1	0.3	0.6	0.6	0.331376
9	−1	0	0	0.1	0.4	0.4	0.295673
10	1	0	0	0.3	0.4	0.4	0.365663
11	0	−1	0	0.2	0.2	0.4	0.330977
12	0	1	0	0.2	0.6	0.4	0.324526
13	0	0	−1	0.2	0.4	0.2	0.319590
14	0	0	1	0.2	0.4	0.6	0.317144
15	0	0	0	0.2	0.4	0.4	0.330705
16	0	0	0	0.2	0.4	0.4	0.330705
17	0	0	0	0.2	0.4	0.4	0.330705
18	0	0	0	0.2	0.4	0.4	0.330705
19	0	0	0	0.2	0.4	0.4	0.330705
20	0	0	0	0.2	0.4	0.4	0.330705

BC are significant factors for local Nu. Consequently, the mathematical Eq. (15) may be rewritten as follows:

$$Nu_x = 0.3304169 + 0.0342968A - 0.0059655B - 0.0014984C + 0.0006833A^2 - 0.0022332B^2 - 0.0116177C^2 - 0.0005710AB + 0.0009227AC - 0.0111890BC. \quad (16)$$

In addition, the values of R-squared, R^2 and adjusted R-squared, and $R^2 - adj$ are shown in Table 4, giving detailed information from the goodness-of-fit of the RSM model. It is noted that Nu is reported with higher R^2 and $R^2 - adj$ values 98.78%, 99.58%, respectively, illustrating a precisely expected correlation between output response variables and independent input variables.

2.2. Sensitivity analysis

As previously mentioned, sensitivity refers to the partial derivation of the response function from the model parameters. As a result, the sensitivity functions of LNN are articulated in relation to governing variables, radiation variable (A), thermophoresis variable (B),

Table 3. ANOVA scrutiny for the LNN.

	Source					
$-\mathrm{Re}_x^{-1/2} Nu_x$	DOF	Sum of square	Contribution	Adj. mean square	F-value	p-value
Model	9	0.013953	99.78%	0.004651	505.3	4.32×10^{-12}
Linear	3	0.012141	86.82%	0.004047	1318.92	0
Square	3	0.000801	5.73%	0.000267	87.02	0
Interaction	3	0.001011	7.23%	0.000337	109.83	0
Residual error	10	0.000031	0.22%	0.000000	–	–
Lack of fit	5	0.000031	0.22%	0.000000	–	–
Pure error	5	0.000000	–	0.000000	–	–
Total	19	0.013984	–	–	–	–

Table 4. Estimated regression coefficients via local N_u.

	Term			
$-\mathrm{Re}_x^{-1/2} Nu_x$	Estimate	Std. error	t-value	p-value
Constant	0.3304169	0.0006022	548.694	2×10^{-16}
A	0.0342968	0.0005539	61.915	2.94×10^{-14}
B	–0.0059655	0.0005539	–10.769	8.03×10^{-7}
C	–0.0014984	0.0005539	–2.705	0.0221
A^2	0.0006833	0.0010563	0.647	0.5323
B^2	–0.0022332	0.0010563	–2.114	0.0606
C^2	–0.0116177	0.0010563	–10.998	6.60×10^{-7}
AB	–0.0005710	0.0006193	–0.922	0.3782
AC	0.0009227	0.0006193	1.490	0.1671
BC	–0.0111890	0.0006193	–18.067	5.78×10^{9}
	$R^2 = 99.78\%$			$R^2 - adj = 99.58\%$

and Brownian motion variable (C) through Eq. (16):

$$\frac{\partial Nu_x}{\partial A} = 0.0342968 + 0.0013666A - 0.0005710B + 0.0009227C,$$

$$\frac{\partial Nu_x}{\partial B} = -0.0059655 - 0.0044664B - 0.0005710A - 0.0005710C,$$

$$\frac{\partial Nu_x}{\partial C} = -0.0014984 - 0.0232354C + 0.0009227A - 0.0111890B.$$

By utilizing Eqs. (17) and (18), the sensitivity findings of the responses (Nu_x) as well as the input governing variables (A, B, and C) are established (see Table 5). A positive degree of sensitivity illustrating the increase in input governing variable causes an increment in the response function, and vice versa, for the negative sensitivity value. The sensitivity inspection results have been plotted into vertical bar charts (Figures 2 and 3) for a more noteworthy insight.

3. Results and discussion

The present statistical analysis attempts to shed light on some significant insights into the stagnant point flow of Walters-B nanoliquid on a radiative Riga surface. To illustrate the significance of the considered problem, the sensitivity analysis of the LNN is investigated based on the relevant parameters. To this end, the parameters of interest including radiation, thermophoresis, and Brownian motion parameter are assumed. In addition, a Bar chart is drawn according to the numerical values of the SFC and LNN.

Table 6 shows the process of a comprehensive analysis in a limited scope when $Q = \beta = 0 = We$. This table points to the high level of acceptance. Table 7 is arranged to analyze the effect of related parameters like We, A, and Q on SFC. It is worth remembering that SFC is reduced for larger We, A , and Q. The influence of We, A, Q, R_d, δ, and Pr on

Table 5. Sensitivity for LNN when $A = -1$.

A	B	C	Sensitivity $\frac{\partial Nu_x}{\partial A}$	Sensitivity $\frac{\partial Nu_x}{\partial B}$	Sensitivity $\frac{\partial Nu_x}{\partial C}$
$A=-1$	-1	-1	0.0325785	-0.0003571	0.0320033
		0	0.0335012	-0.0009281	0.0087679
		1	0.0344239	-0.0014991	-0.0144675
	0	-1	0.0320075	-0.0048235	0.0208143
		0	0.0329302	-0.0053945	-0.0024211
		1	0.0338529	-0.0059655	-0.0256565
	1	-1	0.0314365	-0.0092899	0.0096253
		0	0.0323592	-0.0098609	-0.0136101
		1	0.0332819	-0.0104319	-0.0368455
$A=0$	-1	-1	0.0339451	-0.0009281	0.032926
		0	0.0348678	-0.0014991	0.0096906
		1	0.0357905	-0.0020701	-0.0135448
	0	-1	0.0333741	-0.0053945	0.021737
		0	0.0342968	-0.0059655	-0.0014984
		1	0.0352195	-0.0065365	-0.0247338
	1	-1	0.0328031	-0.0098609	0.010548
		0	0.0337258	-0.0104319	-0.0126874
		1	0.0346485	-0.0110029	-0.0359228
$A=1$	-1	-1	0.0353117	-0.0014991	0.0338487
		0	0.0362344	-0.0020701	0.0106133
		1	0.0371571	-0.0026411	-0.0126221
	0	-1	0.0347407	-0.0059655	0.0226597
		0	0.0356634	-0.0065365	-0.0005757
		1	0.0365861	-0.0071075	-0.0238111
	1	-1	0.0341697	-0.0104319	0.0114707
		0	0.0350924	-0.0110029	-0.0117647
		1	0.0360151	-0.0115739	-0.0350001

Table 6. Comparison of $f''(0)$ through Hayat et al. [50] and Mahapatra and Gupta [51] for $We = \beta = Q = 0$.

A	Current work	Hayat et al. [50]	Mahapatra and Gupta [51]
0.2	-0.91790	-0.91692	-0.9181
0.5	-0.66740	-0.66722	-0.6673
2.0	2.01750	2.01750	2.01750
3.0	4.72920	4.72910	4.72930

LNN is illustrated through Table 8. This table demonstrates that LNN intensifies following the increment in modified Hartman number Q, ratio parameter A, conjugate parameter δ, thermal radiation parameter

Table 7. Numerical values of SFC $\mathrm{Re}_x^{1/2}C_f$ for values of different physical parameters.

$Re_x^{1/2}C_f$	A	We	Q
0.7380	0.2	0.0	0.2
0.5563	–	0.1	–
0.3464	–	0.2	–
0.0957	–	0.3	–
0.5948	0.0	–	–
0.5838	0.1	–	–
0.5563	0.2	–	–
0.5149	0.3	–	–
0.6856	–	–	0.0
0.6196	–	–	0.1
0.5563	–	–	0.2
0.4947	–	–	0.3

Table 8. Values of LNN $\mathrm{Re}_x^{-1/2}Nu_x$ for different physical parameters values.

We	A	Q	R_d	δ	Pr	$-\mathrm{Re}_x^{-1/2}Nu_x$
0.0	0.2	0.2	0.1	0.5	1.0	0.7074
0.1	–	–	–	–	–	0.7009
0.2	–	–	–	–	–	0.6937
0.3	–	–	–	–	–	0.6858
0.1	0.1	0.2	0.1	0.5	1.0	0.6861
–	0.2	–	–	–	–	0.7009
–	0.3	–	–	–	–	0.7154
–	0.4	–	–	–	–	0.7224
0.1	0.2	0.0	0.1	0.5	1.0	0.6657
–	–	0.1	–	–	–	0.6829
–	–	0.2	–	–	–	0.7009
–	–	0.3	–	–	–	0.7176
0.1	0.2	0.2	0.1	0.5	1.0	0.6614
–	–	–	0.2	–	–	0.6998
–	–	–	0.3	–	–	0.7389
–	–	–	0.4	–	–	0.7806
0.1	0.2	0.2	0.1	0.1	1.0	0.7590
–	–	–	–	0.2	–	0.7669
–	–	–	–	0.3	–	0.7773
–	–	–	–	0.4	–	0.7910
0.1	0.2	0.2	0.1	0.5	1.0	0.6992
–	–	–	–	–	1.2	0.7739
–	–	–	–	–	1.3	0.8105
–	–	–	–	–	1.4	0.8471

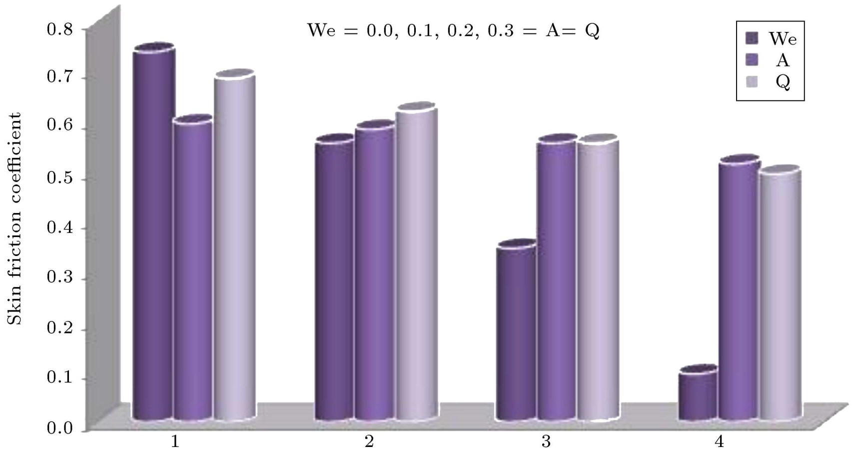

Figure 2. Bar Chart of SFC.

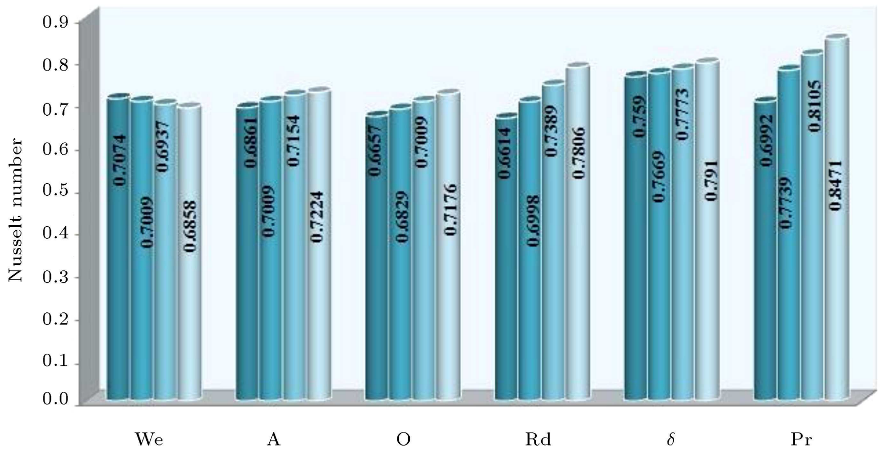

Figure 3. Bar Chart of LNN.

R_d, and Pr although it decreases upon increasing We. Based on the data of skin friction (see Table 7), the bar charts are plotted separately and in combination. Also, a bar chart is drawn for the Nusselt number data, as given in Table 8.

The box plot portrays the distribution dispersion or spread. It makes use of the highest and lowest values for the data, the quartiles (Q_1 and Q_3), and the median Q_2. Figure 4 plots a box plot for Nusselt number responses in the case of Nusselt number and SFC. The SFC is evenly distributed to a greater degree with a smaller range. There is a significant increase in Nusselt number and responses of Nusselt number that are not evenly distributed. The distribution of Nusselt number is positively skewed. Sometimes, high or low values appear in a set of data. The solid points are the extreme values of the SFCs and responses of the Nu. In Figure 5, the residual curves in each response are displayed individually to provide further analysis of the model accuracy. A normal probability plot is very helpful in testing normality assumptions. There are two versions of normal probability plots: $P-P$ and $Q-Q$ plots. It is important to keep in mind that

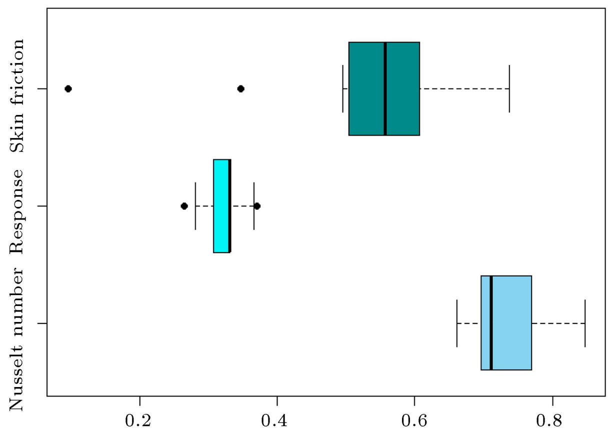

Figure 4. Box plot for Nusselt number, responses of Nusselt number, and Skin friction coefficient.

the normality of the findings is verified by drawing the usual probability plots for residual distribution. With a few exceptions, the usual probability plots for the response are nearly straight lines. This suggests that the regression model fits with the observed values accurately and that the model is valuable and relevant

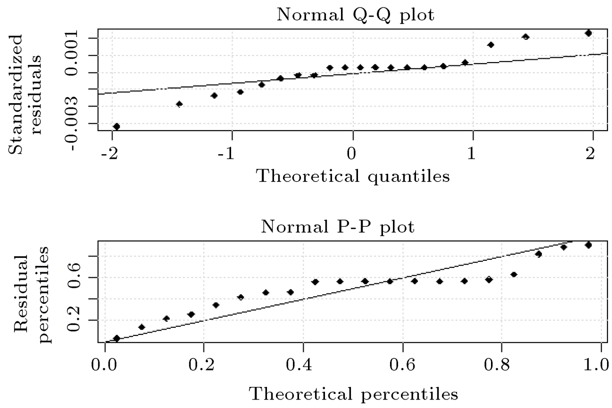

Figure 5. Normal P-P and Q-Q plot of the residuals for the Nusselt number.

enough. Figure 6 shows the density and histogram for residual distribution. It is observed that the residual histogram has a lower degree of skewness and is more similar to a symmetrical distribution.

The findings of the sensitivity analyses are demonstrated with vertical bar charts for a better comprehension (see Figures 7(a)–(c) and 9(a)–(c)). According to this notion, the above and right bar displays a direct sensitivity value, while the inverted bar displays an inverse sensitivity value. As noted earlier, when Figure 7(a)–(c) reveal a general pattern in which the direct sensitivity of LNN (Nu_x) to A (Radiation parameter) rises upon increment in C (Brownian motion number) from -1 to 1. Meanwhile, the sensitivity of LNN to C decreases upon increase in B; however, the sensitivity value also varies from positive to negative for all values of C. As shown in Figure 8(a)–(c), in the case of $A = 0$, we observe that the posit2ive sensitivity of LNN to A (radiation parameter) rises with an increment in C (Brownian motion number) from -1 to 1 and also, for B (thermophoresis number) from -1 to 1. In addition, the sensitivity of LNN to B and C is reduced with an increment in B and also, in the case of C $(-1, 0, 1)$. The sensitivity of LNN to A rises due to an increase in C and also for enhancement B is noted in Figure 9(a)–(c) when $A = 1$.

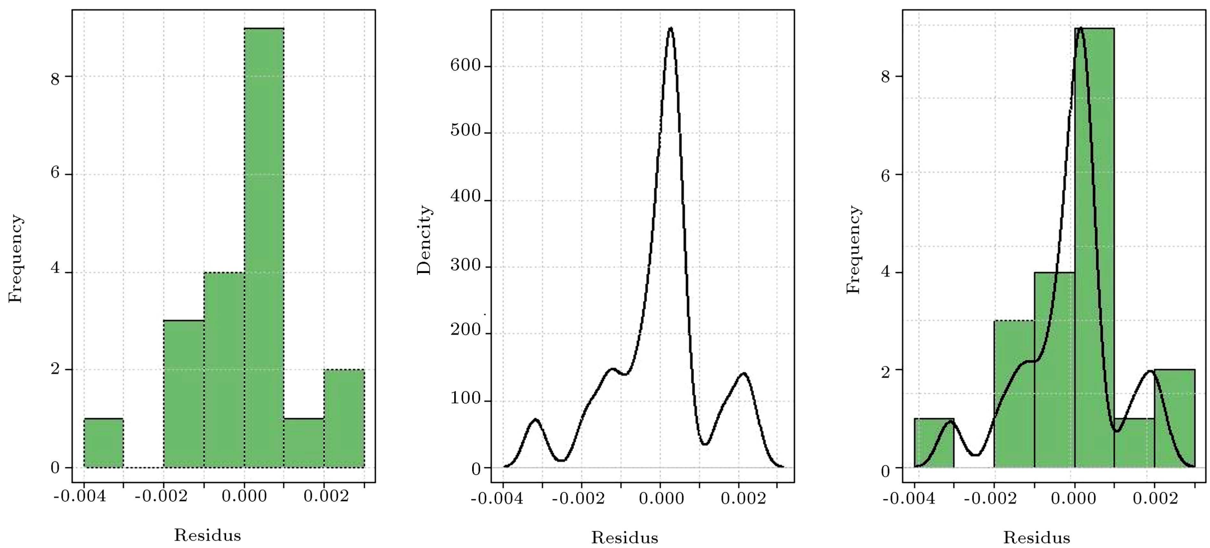

Figure 6. Density and histogram plots of residuals for Nu number.

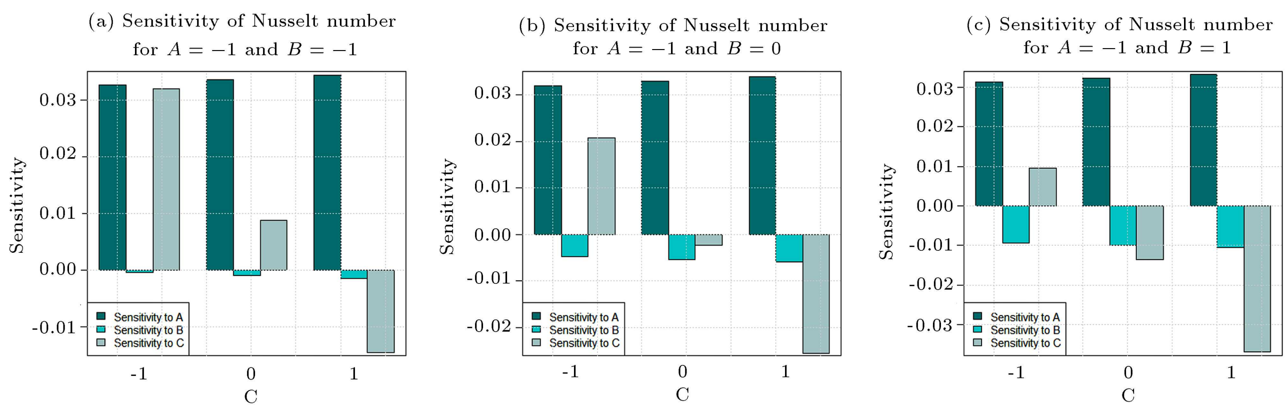

Figure 7. Sensitivity results for LNN when $A = -1$.

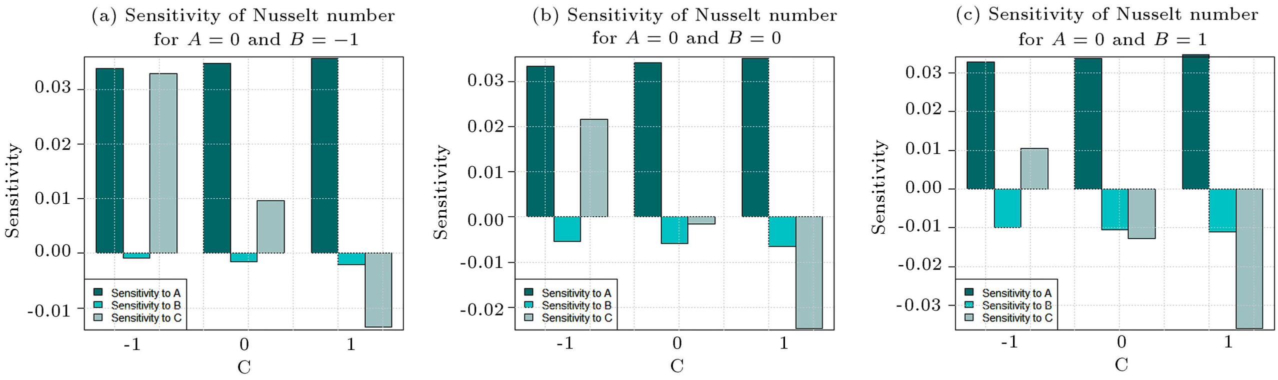

Figure 8. Sensitivity results for LNN when $A = 0$.

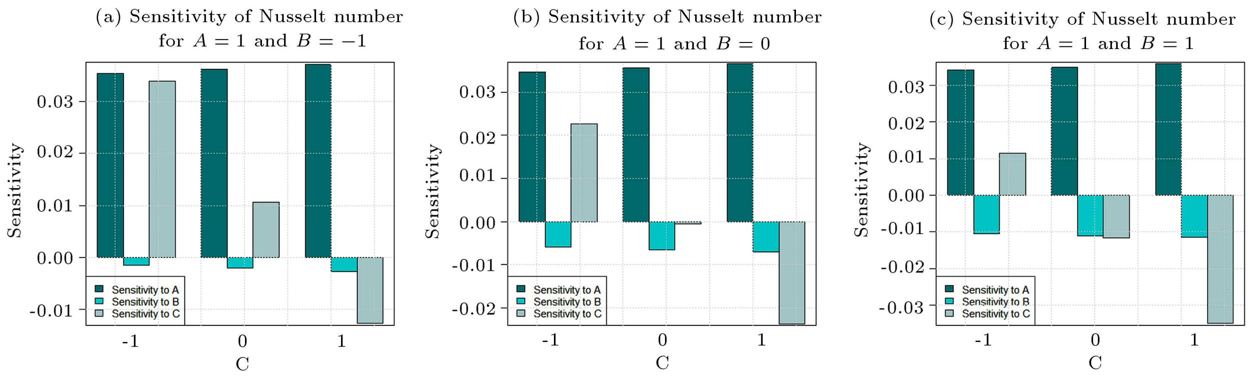

Figure 9. Sensitivity results for LNN when $A = 1$.

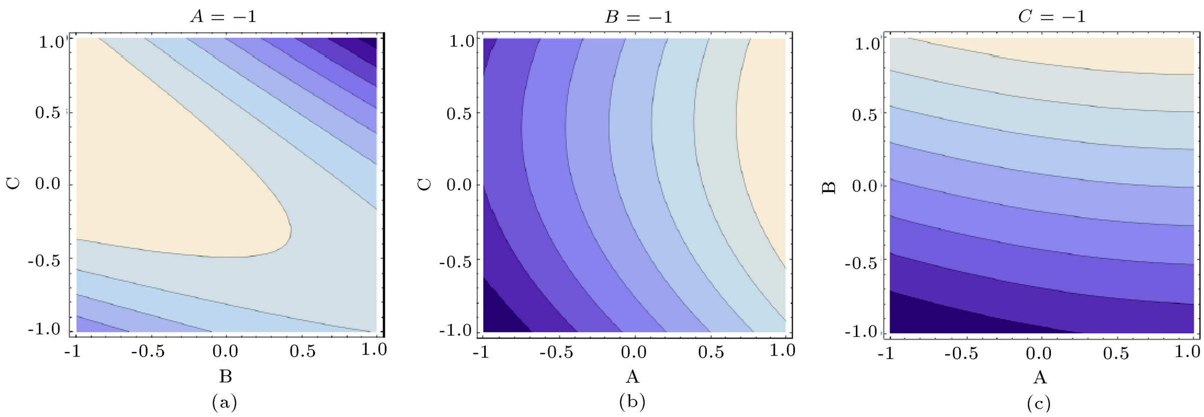

Figure 10. Predicted responses for LNN: (a) B and C, (b) A and C, and (c) A and B.

Figure 10 plots the predicted LNN as a function of radiation (A), thermophoresis (B), and Brownian motion (C) parameters when $A = -1 = C = B$. The impacts of thermophoresis and Brownian number on LNN for $A = -1$ ($R_1 = 0.1$) are given in Figure 10(a). It is to be investigated that the maximum LNN occurs at a higher level of thermophoresis (B) and for Brownian motion (C) parameters. Moreover, the opposite behavior is given in Figure 10(c). In addition, the maximum average LNN occurs in an area closer to the low levels for radiation (A) and Brownian (B) numbers (see Figure 10(b)).

The predicted LNN as a function of radiation (A), thermophoresis (B), and Brownian (C) parameters is given in the case of $A = 0 = B = C$ and $A = 1 = C = B$ in Figures 11 and 12. The impacts of thermophoresis and Brownian motion parameters over LNN for $A = 0$ are given in Figure 11(a). We investigate if the LNN is maximum in a region close to the high level of thermophoresis (B) and Brownian motion (C) variables. For the case of $B = 0$, the maximum LNN is observed when A lies from -1 to -0.5 and C varies from -1 to 1 (see Figure 11(b)). Moreover, in the case of $C = 0$, the maximum

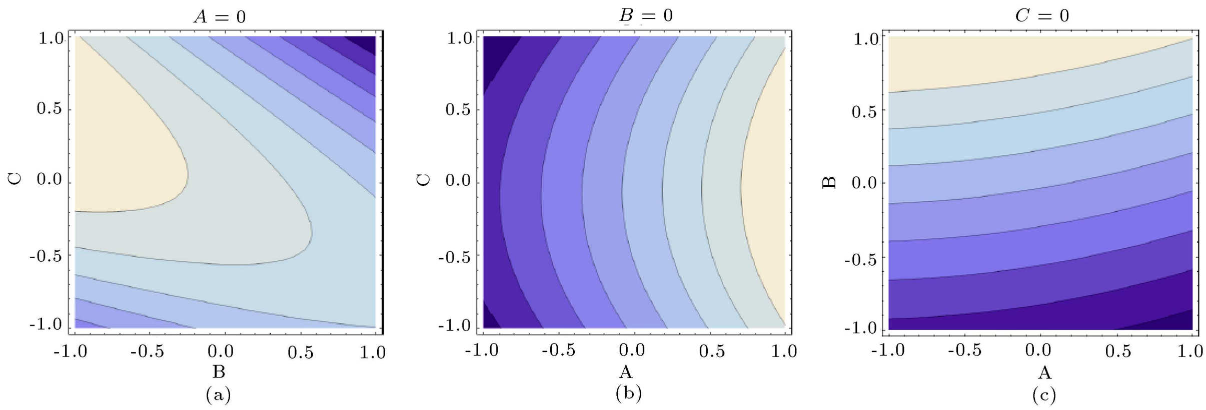

Figure 11. Predicted responses for LNN: (a) B and C, (b) A and C, and (c) A and B.

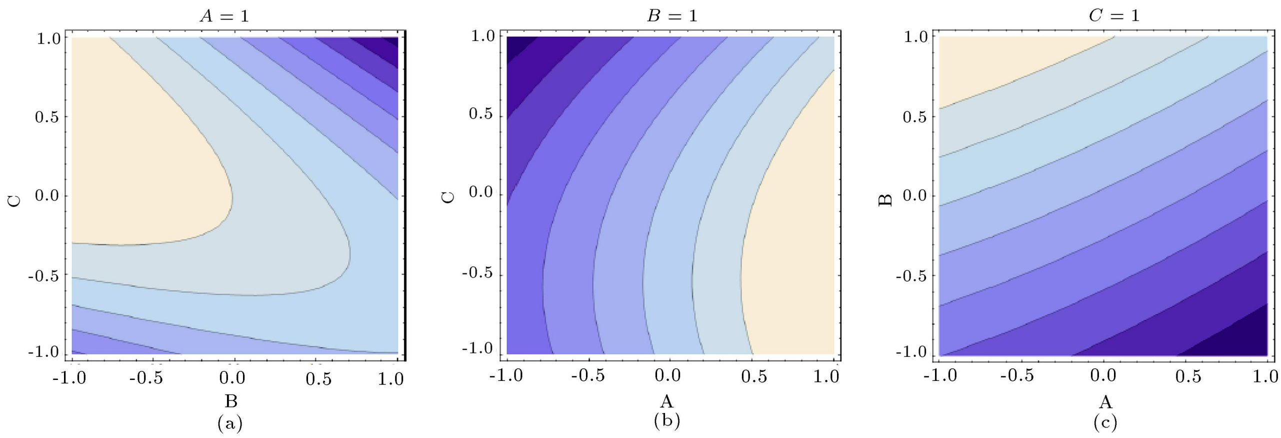

Figure 12. Predicted responses for LNN: (a) B and C (b) A and C and (c) A and B.

average LNN occurs in a region near the low levels for thermophoresis (B) and for all levels of A. The same behavior is observed in Figure 12(a) in comparison to that in Figure 10(a). In the case of $B = 1$, LNN attains the maximum level at higher values of C and lower level of A. Moreover, in the case of high radiation and lower thermophoresis, LNN attains its maximum level for $C = 1$ (see Figure 12 (c)).

4. Conclusions

A numerical analysis of heat transport enhancement corresponding to a sensitivity analysis was performed using response surface strategies to control the Walters-B nanofluid stagnant point flow caused by a Riga surface employing Response Surface Methodology (RSM). The main findings are given below:

- The distribution of Nusselt number was positively skewed;
- Box plot for Nusselt number responses in the case of Nusselt number and skin friction coefficient showed that the skin friction coefficient was more evenly distributed in a smaller range, whereas there was a significant increment in Nusselt number and responses of Nusselt number that were not evenly distributed;
- The normal probability plots $P-P$ and $Q-Q$ residual plot showed the excellent fitted regression model for Local Nusselt Number (LNN);
- The values of the factors A, B, C, B^2, C^2, and BC were significant for the LNN;
- Maximum LNN occurred at the higher values of thermophoresis and Brownian motion parameters;
- Maximum average LNN occurred at lower values of radiation (A) and Brownian (B) numbers;
- Sensitivity of LNN to C decreased with increase in B; however, the sensitivity value also varied from positive to negative for all values of C.

Nomenclature

T	Nanofluid temperature, K
M_0	Magnetization of the permanent magnets mounted on the area of Riga plate
a	Width of the magnets between the electrodes

$\tilde{D}_t s$	Thermophoretic diffusivity coefficient, $m^2 s^{-1}$
j_0	Applied current density in electrodes
$\tilde{H}$	Concentration of nanofluid, mol m^{-3}
C_w	Wall's nanoparticle volume fraction, mol m^{-3}
C_∞	Ambient concentration, mol m^{-3}
$\tilde{D}_b$	Brownian diffusivity coefficient, m^2 s^{-1}
c_p	Heat at uniform pressure, Kg^{-1} J K^{-1}
R_d	Radiation parameter
K	Thermal conductivity, Kg m s^{-3} K^{-1}
N_1	Thermophoresis parameter
Pr	Prandtl number
T_w	Wall's temperature, K
(x, y)	Coordinate system
q_r	Radiative flux
k_1	Mean absorption coefficient
(u, v)	Velocity components, m s^{-1}
q_r	Radiative flux, W m^{-2}
S_c	Schmidt number
T_∞	Ambient fluid's temperature, K
U_e	Free stream velocity
δ	Conjugate term
Q_1	Modified Hartman number
N_2	Brownian motion parameter
β	Dimensionless parameter
W_e	Weissenberg number
A	Ratio parameter

Greek symbols

μ	Dynamic viscosity of base liquid, kg m^{-1} s^{-1}
$\tilde{\tau}$	Fraction of effective heat capacity
ϕ	Non-dimensional concentration
σ^*	Stefan-Boltzmann constant
α	Fluid thermal diffusivity, m s^{-1}
σ	Electrical conductivity, Ω^{-1} m^{-1}
ρ	Density of liquid, kg m^{-3}
η	Similarity variable
θ	Nondimensional temperature
$\tilde{\sigma}^*$	Coefficient of mean adsorption
ν	Dynamic viscosity, m^2 s^{-1}

Abbreviation

LNN	Local Nusselt Number
RSM	Response Surface Methodology
SFC	Skin Friction Coefficient

References

1. Pordanjani, A.H., Vahedi, S.M., Rikhtegar, F., et al. "Optimization and sensitivity analysis of magneto-hydrodynamic natural convection nanofluid flow inside a square enclosure using response surface methodology", *J. Therm. Anal. Calorim.*, **135**, pp. 1031–1045 (2019). https://doi.org/10.1007/s10973-018-7652-6

2. Marzougui, S., Mebarek-Oudina, F., Assia, A. et al. "Entropy generation on magneto-convective flow of copper-water nanofluid in a cavity with chamfers", *J. Therm. Anal. Calorim.*, **143**(3), pp. 2203–2214 (2021). https://doi.org/10.1007/s10973-020-09662-3

3. Rajashekhar, C., Mebarek-Oudina, F., Vaidya, H., et al. "Mass and heat transport impact on the peristaltic flow of Ree-Eyring liquid whit variable properties for hemodynamic flow", *Heat Transfer*, **50**(5), pp. 5106–5122 (2021). https://doi.org/10.1002/htj.22117

4. Mebarek-Oudina, F. "Convective heat transfer of titania nanofluids of different base fluids in cylindrical annulus with discrete heat source", *Heat Transfer*, **48**, pp. 135–147 (2019).

5. Dehkordi, K.S., Fazilati, M.A., and Hajatzadeh, A. "Surface scraped heat exchanger for cooling newtonian fluids and enhancing its heat transfer characteristics, a review and a numerical approach", *Applied Thermal Engineering*, **87**, pp. 56–65 (2015).

6. Mebarek-Oudina, F., Bessaih, R., Mahanthesh, B., et al. "Magneto-thermal-convection stability in an inclined cylindrical annulus filled with a molten metal", *International Journal of Numerical Methods for Heat & Fluid Flow*, **31**(4), pp. 1172–1189 (2021). https://doi.org/10.1108/HFF-05-2020-0321

7. Choi, S.U. and Eastman, J.A. "Enhancing thermal conductivity of fluids with nanoparticles", No. ANL/MSD/CP-84938, CONF-951135–29 (Argonne National Lab., IL, 1995). https://www.osti.gov/servlets/purl/196525

8. Swain, K., Mebarek-Oudina, F., and M.Abo-Dahab, S. "Influence of MWCNT/Fe_3O_4 hybrid-nanoparticles on an exponentially porous shrinking sheet with chemical reaction and slip boundary conditions", *J. Therm. Anal. Calorim.*, **147**, pp. 1561–1570 (2022). https://doi.org/10.1007/s10973-020-10432-4

9. Shafiq, A., Mebarek-Oudina, F., Sindhu, T.N. et al. "A study of dual stratification on stagnation point Walters'B nanofluid flow via radiative Riga plate: a statistical approach", *Eur. Phys. J. Plus*, **136**, p. 407 (2021). https://doi.org/10.1140/epjp/s13360-021-01394-z

10. Jabeen, S., Hayat, T., and Alsaedi, A. "Entropy generation optimization and activation energy in flow of Walters-B nanomaterial", *Scientia Iranica*, **28**(3), pp. 1917–1925 (2021).

11. Abu-Nada, E. "Simulation of heat transfer enhance-

ment in nanofluids using dissipative particle dynamics", Int. *Communications in Heat and Mass Transfer*, **85**, pp. 1–11 (2017).

12. Zaim, A., Aissa, A., Mebarek-Oudina, F., et al. "Galerkin finite element analysis of magneto-hydrodynamic natural convection of Cu-water nanoliquid in a baffled U-shaped enclosure", *Propulsion and Power Research*, **9**(4), pp. 383–393 (2020). https://doi.org/10.1016/j.jppr.2020.10.002

13. Dadheech, P.K., Agrawal, P., Mebarek-Oudina, F., et al. "Comparative heat transfer analysis of $MoS_2/C_2H_6O_2$ and MoS_2- SiO_2/ $C_2H_6O_2$ nanofluids with natural convection and inclined MHD", *Journal of Nanofluids*, **9**(3), pp. 161–167 (2020). https://doi.org/10.1166/jon.2020.1741

14. Chabani, I., Mebarek Oudina, F., and Ismail, A.I. "MHD flow of a hybrid nano-fluid in a triangular enclosure with zigzags and an elliptic obstacle", *Micromachines*, **13**(2), p. 224 (2022). https://doi.org/10.3390/mi13020224

15. Khan, U., Zaib, A., and Mebarek-Oudina, F. "Mixed convective magneto flow of SiO_2-$MoS_2/C_2H_6O_2$ hybrid nanoliquids through a vertical stretching/shrinking wedge: Stability analysis", *Arab. J. Sci. Eng.*, **45**, pp. 9061–9073 (2020). https://doi.org/10.1007/s13369-020-04680-7

16. Shafiq, A., Rasool, G., and Khalique, C.M. "Significance of thermal slip and convective boundary conditions in three dimensional rotating Darcy-Forchheimer nanofluid flow, *Symmetry*, **12**(5), p. 741 (2020).

17. Abo-Dahab, S.M., Abdelhafez, M.A., Mebarek-Oudina, F., et al. "MHD casson nanofluid flow over nonlinearly heated porous medium in presence of extending surface effect with suction/injection", *Indian J. Phys.*, **95**, pp. 2703–2717 (2021). https://doi.org/10.1007/s12648-020-01923-z

18. Selimefendigil, F. and öztop, H.F. "Mixed convection in a partially heated triangular cavity filled with nanofluid having a partially flexible wall and internal heat generation", *J. Taiwan Inst. Chemical Engineers*, **70**, pp. 168–178 (2017).

19. Mebarek-Oudina, F. "Numerical modeling of the hydrodynamic stability in vertical annulus with heat source of different lengths", *Engineering Science and Technology*, **20**(4) pp. 1324–1333 (2017). http://dx.doi.org/10.1016/j.jestch.2017.08.003

20. Das, S.K., Choi, S.U.S., and Patel, H.E. "Heat transfer in nanofluids-a review", *Heat Transfer Engineering*, **27**(10), pp. 3–19 (2006), https://doi.org/10.1080/01457630600904593

21. Buongiorno, J. "Convective Transport in Nanofluids", *J. Heat Transfer*, **128**, pp. 240–250 (2006).

22. Daungthongsuk, W. and Wongwises, S. "A critical review of convective heat transfer of nanofluids", *Renewable and Sustainable Energy Reviews*, **11**(5), pp. 797–817 (2007).

23. Mebarek-Oudina, F., Reddy, N., and Sankar, M. "Heat source location effects on buoyant convection of nanofluids in an annulus", *Advances in Fluid Dynamics, Lecture Notes in Mechanical Engineering*, pp. 923–937 (2021). https://doi.org/10.1007/978-981-15-4308-1_70

24. Pushpa, B.V., Sankar, M., and Mebarek-Oudina, F. "Buoyant convective flow and heat dissipation of Cu-H_2O, nanoliquids in an annulus through a thin baffle", *Journal of Nanofluids*, **10**(2), pp. 292–304 (2021). https://doi.org/10.1166/jon.2021.1782

25. Marzougui, S., Mebarek-Oudina, F., Magherbi, M., et al. "Entropy generation and heat transport of Cu-water nanoliquid in porous lid-driven cavity through magnetic field", *International Journal of Numerical Methods for Heat & Fluid Flow* (2021). https://doi.org/10.1108/HFF-04-2021-0288

26. Atif, S.M., Hussain, S., and Sagheer, M. "Effect of thermal radiation on MHD micropolar Carreau nanofluid with viscous dissipation, Joule heating, and internal heating", *Scientia Iranica*, **26**(6), pp. 3875–3888 (2019).

27. Jabeen, S., Hayat, T., Alsaedi, A., et al. "Consequences of activation energy and chemical reaction in radiative flow of tangent hyperbolic nanoliquid", *Scientia Iranica*, **26**(6), pp. 3928–3937(2019).

28. Warke, A.S., Ramesh, K., Mebarek-Oudina, F., et al. "Numerical investigation of nonlinear radiation with magnetomicropolar stagnation point flow past a heated stretching sheet", *Journal of Thermal Analysis and Calorimetry* (2021). https://doi.org/10.1007/s10973-021-10976-z

29. Mebarek-Oudina, F., Fares, R., Aissa, A., et al. "Entropy and convection effect on magnetized hybrid nano-liquid flow inside a trapezoidal cavity with zigzagged wall", *International Communications in Heat and Mass Transfer*, **125**, p. 105279 (2021). https://doi.org/10.1016/j.icheatmasstransfer.2021.105279

30. Djebali, R., Mebarek-Oudina, F., and Choudhari, R. "Similarity solution analysis of dynamic and thermal boundary layers : further formulation along a vertical flat plate", *Physica Scripta*, **96**(8), p. 085206 (2021). https://doi.org/10.1088/1402-4896/abfe31

31. Mebarek-Oudina, F., Aissa, A., Mahanthesh, B., et al. "Heat transport of magnetized newtonian nanoliquids in an annular space between porous vertical cylinders with discrete heat source", *International Communications in Heat and Mass Transfer*, **117**, p. 104737 (2020). http://dx.doi.org/10.1016/j.icheatmasstransfer.2020.104737

32. Shafiq, A., Rasool, G., Khalique C.M., et al. "Second grade bioconvective nanofluid flow with buoyancy effect and chemical reaction", *Symmetry*, **12**(4), p. 621 (2020).

33. Swain, K., Mahanthesh B., and Mebarek-Oudina, F. "Heat transport and stagnation-point flow of magnetized nanoliquid with variable thermal conductivity with Brownian moment and thermophoresis aspects", *Heat Transfer*, **50**(1), pp. 754–764 (2021). https://doi.org/10.1002/htj.21902

34. Gailitis, A. and Lielausis, O. "On a possibility to reduce the hydrodynamic resistance of a plate in an electrolyte", *Appl. Magnetohydrodyn.*, **12**, pp. 143–146 (1961).

35. Ahmad, A., Asghar, S., and Afzal, S. "Flow of nanofluid past a Riga plate", *J. Magn. Magn. Mater.*, **402**, pp. 44–48 (2016).

36. Dhif, K., Mebarek-Oudina, F., Chouf, S., et al. "Thermal analysis of the solar collector cum storage system using a hybrid-nanofluids", *Journal of Nanofluids*, **10**(4), pp. 634–644 (2021). https://doi.org/10.1166/jon.2021.1807

37. Abbas, T., Hayat, T., Ayub, M., et al. "Electromagnet hydrodynamic nanofluid flow past a porous Riga plate containing gyrotactic microorganism", *Neural Comput. Appl.*, **31**(6), pp. 1905–1913 (2019).

38. Nadeem, S., Ahmad, S., and Khan, M.N. "Mixed convection flow of hybrid nanoparticles along a Riga surface with Thomson and Troian slip condition", *J. Therm. Anal. Calorim.*, **143**, pp. 2099–2109 (2021). https://doi.org/10.1007/s10973-020-09747-z.

39. Ganesh, N.V., Qasem, M.A., Sara, A.F., et al. "Riga - plate flow of γ Al_2O_3-water/ethylene glycol with effective Prandtl number impacts", *Heliyon*, **5**(5), e01651 (2019).

40. Rasool, G., Zhang, T., and Shafiq, A. "Second grade nanofluidic flow past a convectively heated vertical Riga plate", *Physica Scripta*, **94**(12), p. 125212 (2019).

41. Shafiq, A., Rasool, G., Phali, L., et al. "Thermosoluted marangoni convective flow towards a permeable riga surface", *Open Physics*, **18**(1) pp. 535–544 (2020).

42. Zhang, L., Bhatti, M.M., Ellahi, R., et al. "Oxytactic microorganisms and thermo-bioconvection nanofluid flow over a porous Riga plate with Darcy-Brinkman-Forchheimer medium", *J. Non Equilib. Thermodyn.*, **45**(3), pp. 257–268 (2020).

43. Bhatti, M.M. and Michaelides, E.E. "Study of Arrhenius activation energy on the thermo-bioconvection nanofluid flow over a Riga plate", *J. Therm. Anal. Calorim.*, **143**, pp. 2029–2038 (2021). https://doi.org/10.1007/s10973-020-09492-3

44. Shafiq, A., Zari, I., Khan, T.S., Khan, et al. "Marangoni driven boundary layer flow of carbon nanotubes towards a riga plate", *Frontiers in Physics*, **7**, p. 215 (2019).

45. Shirvan, K.M., Mamourian, M., Mirzakhanlari, S., et al. "Two phase simulation and sensitivity analysis of effective parameters on combined heat transfer and pressure drop in a solar heat exchanger filled with nanofluid by RSM", *Journal of Molecular Liquids*, **220**, pp. 888–901 (2016). https://doi.org/10.1016/j.molliq.2016.05.031

46. Akbarzadeh, M., Rashidi, S., Bovand, M., et al. "A sensitivity analysis on thermal and pumping power for the flow of nanofluid inside a wavy channel", **220**, pp. 1–13 (2016). https://doi.org/10.1016/j.molliq.2016.04.058

47. Bovand, M., Valipour, M.S., Dincer K., et al. "Application of response surface methodology to optimization of a standard ranque-hilsch vortex tube refrigerator", *Applied Thermal Engineering*, **67**(1–2) pp. 545–553 (2014). https://doi.org/10.1016/j.applthermaleng.2014.03.039

48. Rashidi, S., Bovand, M., and Esfahani, J.A. "Structural optimization of nanofluid flow around an equilateral triangular obstacle", *Energy*, **88**, pp. 385–398 (2015). https://doi.org/10.1016/j.energy.2015.05.056

49. Shafiq, A., Sindhu, T.N., and Khalique, C.M. "Numerical investigation and sensitivity analysis on bio convective tangent hyperbolic nanofluid flow towards stretching surface by response surface methodology", *Alexandria Engineering Journal*, **59**(6), pp. 4533–4548 (2020).

50. Hayat, T., Shafiq, A., Imtiaz, M., et al. "Impact of melting phenomenon in the Falkner-Skan wedge flow of second grade nanofluid: A revised model", *Journal of Molecular Liquids*, **215**, pp. 664–670 (2016).

51. Mahapatra, T. and Gupta, A. "Heat transfer in stagnation-point flow towards a stretching sheet", *Heat and Mass Transfer*, **38**, pp. 517–521 (2002).

Biographies

Anum Shafiq is currently an Associate Professor at the School of Mathematics and Statistics, Nanjing University of Information Science and Technology, China. She received her PhD in 2016 from Quaid-i-Azam University Islamabad, Pakistan. Then, she became an Assistant Professor. She did postdoctoral research from the year 2019 to Jan 2020 at North West University, South Africa. She has published over 83 SCI papers and three book chapters. Her research is mostly focused on numerical methods for boundary value problems, Newtonian and non-Newtonian nanofluid and microorganisms, etc. She is a potential reviewer of top-ranking research journals with a research h-index of over 30 and citations over 2280 as per Web of Sciences.

Fateh Mebarek Oudina received PhD in 2010. He has published more than 100 papers in international journals and proceeding. Currently, he works at Skikda University in Algeria and serves as a reviewer for more than 200 indexed international journals. His name was included in the two last American Stanford University lists "Top 2% Best Scientists in the World".

Tabassum Naz Sindhu received her MPhil degree in Statistics from Quaid-i-Azam University, Islamabad, Pakistan. She is currently working at various universities for teaching including Quaid-i-Azam University, National University of Computer & Emerging Sciences, and International Islamic University, Islamabad. Her research interests concern mathematical and computational methods in statistics, distribution theory with applications to real-life data, sensitivity analysis, response surface methodology, etc.

Ghulam Rasool has received PhD in Applied Mathematics from one of the world's leading Universities, Zhejiang University, China. He is currently affiliated with Wuxi University as an Assistant Professor of Mathematics. His research includes the areas of fluid dynamics, MHD flows, nanofluids, theoretical physics, differential equations, and mathematical modeling of real-world problems. He is a potential reviewer of top-ranking research journals with a research index over 20 and over 900 citations as per Web of Science.